Int J Adv Manuf Technol (2012) 59:119–126
DOI 10.1007/s00170-011-3497-x

ORIGINAL ARTICLE

# Assessment of machining performance using the wear map approach in micro-drilling

**Muhammad Imran · Paul T. Mativenga · Philip J. Withers**

Received: 25 November 2010 / Accepted: 26 June 2011 / Published online: 19 August 2011


**Abstract** It is well established that nickel-based super alloys exhibit poor machinability. One of the challenges in micro-drilling of these alloys is to increase productivity while maintaining acceptable tool wear rates. In this regard, the wear map approach is a useful way to identify an operating window of cutting conditions. The progression of tool wear has been studied in relation to tool edge radius and undeformed chip thickness. A characteristic wear map of cutting conditions is constructed for the micro-drilling process. This helps identify the zones of lowest wear rate, commonly referred to as safe zones, as well as a scale effect in the micro-domain. The new wear rate map provides a quick and useful reference for selecting suitable cutting conditions with the aim of reducing manufacturing costs and/or increasing production rate for micro-drilling. A preliminary tool wear mechanism study suggests that abrasion, adhesion and micro-chipping are the active tool wear modes associated with wet micro-drilling of nickel-based super alloys.

**Keywords** Wear map · Drilling · Wear mechanism · Machining · Micro-machining · Tool life

M. Imran (✉) · P. T. Mativenga
Manufacturing and Laser Processing Research Group,
School of Mechanical, Aerospace and Civil Engineering,
The University of Manchester,
Sackville St,
M13 9PL Manchester, UK
e-mail: muhammad.imran.umist@gmail.com

P. J. Withers
School of Materials, The University of Manchester,
Grosvenor St,
M1 7HS Manchester, UK

## 1 Introduction

It is well established that nickel alloys have poor machinability due to a combination of high temperature strength and low thermal conductivity [1–4]. Precipitate hardening arising from the $\gamma''$ secondary phase ($Ni_3Nb$), together with rapid work-hardening [5] contribute to the high yield and tensile strengths of the material [3, 4, 6, 7]. The potential for reaction with the tool material and the presence of hard abrasive particles in the microstructure further exacerbate the machining difficulties.

For almost all machining operations, tool wear is a critical aspect with respect to the productivity and quality of the machined surface. With regard to productivity, a wear map is a useful means of identifying suitable parameters across the feed/speed plane. Safety zones can be identified as regions which provide the lowest tool wear rates. The tool wear can simply be defined as a plane on which normalised wear rate parameters are plotted. The use of wear maps becomes especially important in the machining of difficult-to-cut nickel-based super alloys where improper conditions could significantly increase component cost and reduce productivity.

The potential of wear maps was first realised by Lim et al. in 1987, implementing both empirical and experimental approaches to characterise the wear between the sliding surfaces in steels [8]. Later, this framework was extended to aluminium alloys [9] as well as for the dry turning of steels using uncoated high speed steel (HSS) tools [10]. The fact that the work-piece material could strongly affect the wear map was later recognised by Lim and co-workers [11, 12] for dry turning operations. Wear maps have also developed for the turning of Ti-6Al-4V alloy using uncoated carbide tools to identify the presence of safety zones [13]. With regard to the hole-making process using a micro-end-mill, Lee and Dornfeld [14] constructed contour maps for the prediction of burr size and tool life for SS304 steel. For

drilling, tool wear maps and the associated mechanisms were first identified for the machining of aluminium [15] and magnesium alloys [16] using uncoated HSS tools. However, wear maps for the machining of nickel-based super alloys have not been reported to date. The definition of wear maps for the drilling of nickel-based super alloys would provide a useful tool for industry in identifying drilling parameters giving low wear rates. This is also true for micro-drilling for which it is important to recognise the tool wear characteristics at low to high feed/speed ranges as well as to reduce the cycle times for the micro-drilling process as compared with existing electrical discharge machining (EDM) process in turbine blade applications.

In addition to the developing a wear map, it is essential that the associated tool wear mechanisms are identified. In this regard, studies have been conducted for macro- [7, 17] and micro-drilling [18–20]. However, the variations of tool wear over a broad feed and speed envelope have not been investigated for the micro-drilling of nickel-base super alloys. This is partly because of the difficulty in measuring micro-tools. Furthermore, there are scale-related issues associated with micro-machining which can compromise tool life [18, 21–24]. Take for example, for micro-drilling, the small undeformed chip thickness; tool flank face rubbing arising from elastic recovery of the work-piece and ploughing caused by the tool edge radius become important mechanisms of energy dissipation [25–27]. All these factors can directly influence the tool life. Consequently, it is important to identify the dominant tool wear modes at various cutting speeds and feed-rates.

### 1.1 Feed, speed and size-effects

Cutting conditions play a critical role in determining the cutting performance in any machining process. As for conventional machining, cutting speed, feed and depth of cut cannot be downscaled into the micro-range due to scale effects [21]. Feed was found to be the dominant parameter in the micro-drilling process as it determines the chip thickness and resulting cutting force [14]. The value of feed is influenced not only by the flow and intensity of the cutting effects but also the quality of the hole [28]. No guide figures were available to determine the feed values in micro-cutting of this super alloy. High feed-rates may disable the cutting process, and this is usually associated with excessive tool wear or drill breakage. On the other hand, very low feed rates could imply that the process is below the minimum chip thickness. Thus, the minimum chip thickness and drill brakeage set the theoretical limits of the feed-rate window for micromachining.

One of the main differences between micro-cutting and conventional cutting is the cutting speed range [14]. The cutting speeds in micro-machining domain are far lower than for conventional machining, especially for workpiece materials having low thermal conductivity [29]. For instance, in conventional machining, the cutting speed range for machining of nickel super alloys varies from 10–300 m/min [30]. For a 0.5-mm drill, if a cutting speed of 100 m/min was required, then the spindle speed would be 64,000 rpm. This RPM is beyond the spindle speeds of most machines. However, initial tests were conducted at higher spindle speeds of 20,000; 30,000 and 40,000 rpm on the nickel-based super alloy. The drills were easily fractured at such high cutting speeds. Therefore, a lower range of cutting speed was used as recommended in a previous study [18]. This shows that, for nickel alloys, the cutting speeds used in micro-machining are generally orders of magnitude slower than for conventional high-speed macro-scale machining.

In addition to feed and speed, another parameter of interest in micro-machining is the ratio of the feed to the cutting edge radius of the tool [31]. This ratio affects the rake angle, specific energy and, ultimately, the micro-machining performance. Using a lower feed in relation to the tool edge radius could lead to highly negative effective rake angles and therefore promote ploughing and plastic deformation phenomena during drilling.

## 2 Experimental details

### 2.1 Workpiece material

Micro-drilling tests were carried out on rectangular 2.2-mm-thick flat plates of nickel-based super alloy, Inconel 718 alloy, from a wrought condition and annealed at 954–982°C. The material was supplied by Goodfellow Cambridge Limited England, UK having the nominal chemical composition (wt.%) of Ni ~52.5%, Cr ~19%, Fe ~18.5%, Mo ~3%, Nb+Ta ~5.13%, Ti ~0.9% and Al ~0.5%. The average (approximately equi-axed) grain size of the parent material was found to be 12 μm from the analysis of electron backscatter diffraction (EBSD) maps. EBSD measurements were taken on a high-resolution field emission gun (FEG) Philips XL 30 FEG-SEM at a working distance of 20 mm and accelerating voltage of 20 kV. Channel-5 software from HKL technology was used to analyse the EBSD measurements. A backscatter electron (BSE) photomicrograph of the parent material microstructure is shown in Fig. 1. The average hardness of the parent material was calculated to be 3.67 GPa from a number of measurements recorded using a MTS XP Nano Instruments, USA, nano-indenter.

### 2.2 Micro-drilling tests

Drilling tests were conducted using a Mikron HSM 400 high-speed machining centre having a maximum spindle speed of 42,000 rpm. A twist drill of 500 μm diameter was

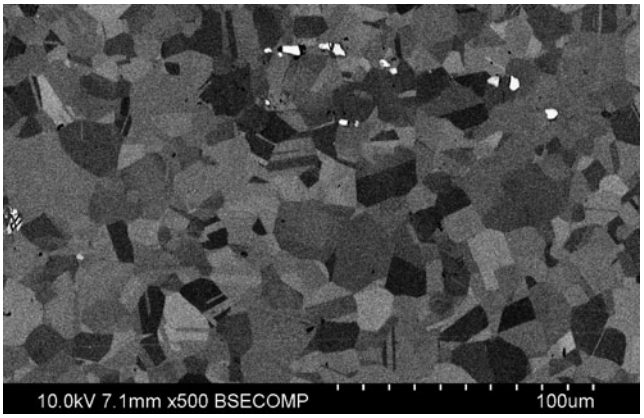


**Fig. 1** Backscatter electron (BSE) photomicrograph of parent material microstructure

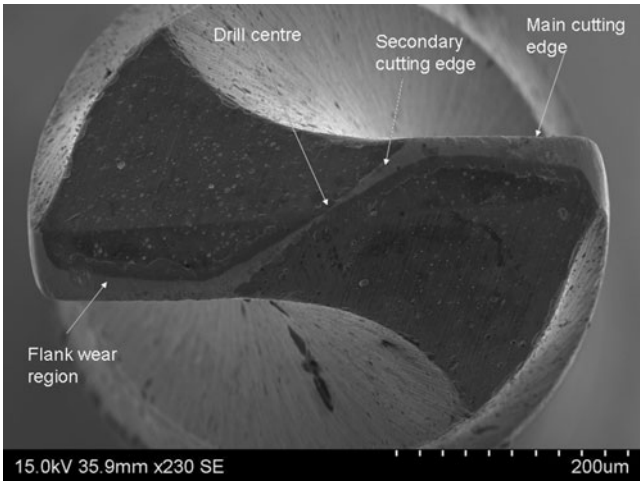


**Fig. 3** Twist drill showing wear at the main cutting edge, secondary cutting edge and drill centre

employed for the cutting tests. This twist drill had a higher point angle (150°) than a standard twist drill which has a 118° point angle. A previous geometry study showed that increasing the point angle to 150° could result in enhanced drill life [19]. Additionally, the drill had a high web thickness (32% of the diameter) to provide high torsional rigidity to the tool [32]. The cutting strategy focused on centre and twist drills having different point angles, i.e., 120° for centre drill and 150° for twist drill, as recommended by a previous study [18]. The representative tool geometry of the twist drill is shown in Fig. 2.

The TiN-coated drills were made from ultra-fine tungsten carbide having 8 wt.% cobalt binder. The grain size of the drill material was measured and found to be in the range of 500–600 nm. The hardness was found to be 23 GPa on average. These drills are made with a shank of 3 mm diameter. The average edge radius was measured to be 3.5 μm from high magnification images taken by a scanning electron microscope (SEM). The SEM images were imported into AUTOCAD software, followed by fitting circles on the cutting edges. The radius of the best-fit circle was taken as the tool edge radius. This edge radius is a determining factor in order to identify the effective rake angle and in analyzing the cutting mode, i.e., shearing and ploughing. In the cutting tests, the tool overhang was kept constant. Through holes were machined in the plates.

Cutting tests with flood coolant were conducted using Hocut 3830 water-based coolant. The cutting conditions were based on an earlier study with the feed-rate varying from 0.5–11 μm/rev and the cutting speed from 1.57–17.27 m/min with a peck depth of 0.1 mm [18].

Tool flank wear (VB) and the main cutting edge radius ($r_e$) were monitored at small intervals during the process. The cutting edge measurements were taken by SEM after drilling holes at predefined time intervals. The drill was taken from the machine, measured and then used to continue drilling to the next time interval.

The wear map was plotted after making 58 holes on the specimen. In order to check the repeatability of results, a second new drill was used to repeat each of the cutting conditions. The data reported is an average value of the two readings. All the studies for tool wear were carried out on a Hitachi 3400 SEM at 8–20 kV accelerating voltage. Energy dispersive X-ray (EDX) measurements were taken on Carl Zeiss EVO 50 SEM at accelerating voltage of 20 kV. A two-dimensional flank wear map was constructed by employing

**Fig. 2** Cutting geometry for the 500 μm diameter twist drill

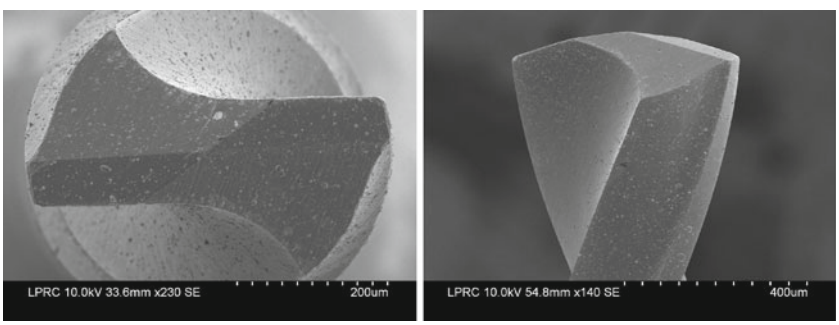


(a) Top view (b) Side view

the speed as abscissa and feed-rate as ordinate. A dimensionless wear parameter, $R$, which denotes a wear per unit cutting length as defined in literature [16], was plotted on the wear map. This was calculated using the parameter log(VB/$L$), where $L$ is the cutting distance.

## 3 Results and discussion

### 3.1 Tool wear phenomena

Figure 3 shows representative tool wear on a twist drill after making 58 holes. Tool wear can be seen to occur near the main cutting edges, secondary cutting edges and drill centre. Tool wear was measured on the main cutting edges of the flank face.

Figure 4a shows flank wear progression of a tool for an increasing number of holes drilled over the entire cutting period (400 holes). The cutting speed and feed-rate were 4.7 m/min (3000 rpm) and 5 μm/rev, respectively. The evolution of tool wear was found to follow the classical three-stage process [33]. During the first couple of holes, in stage-1, the tool wears (Fig. 4b) rapidly, as represented by a high slope in Fig. 4a. During stage-2, the tool wear (Fig. 4c) was steadily increased, indicated by a lower slope in the flank wear curve than for stage-1. Stage-3 can be characterised by rapid increase in tool wear (Fig. 4d) after 350 holes. This stage is characterised by significant

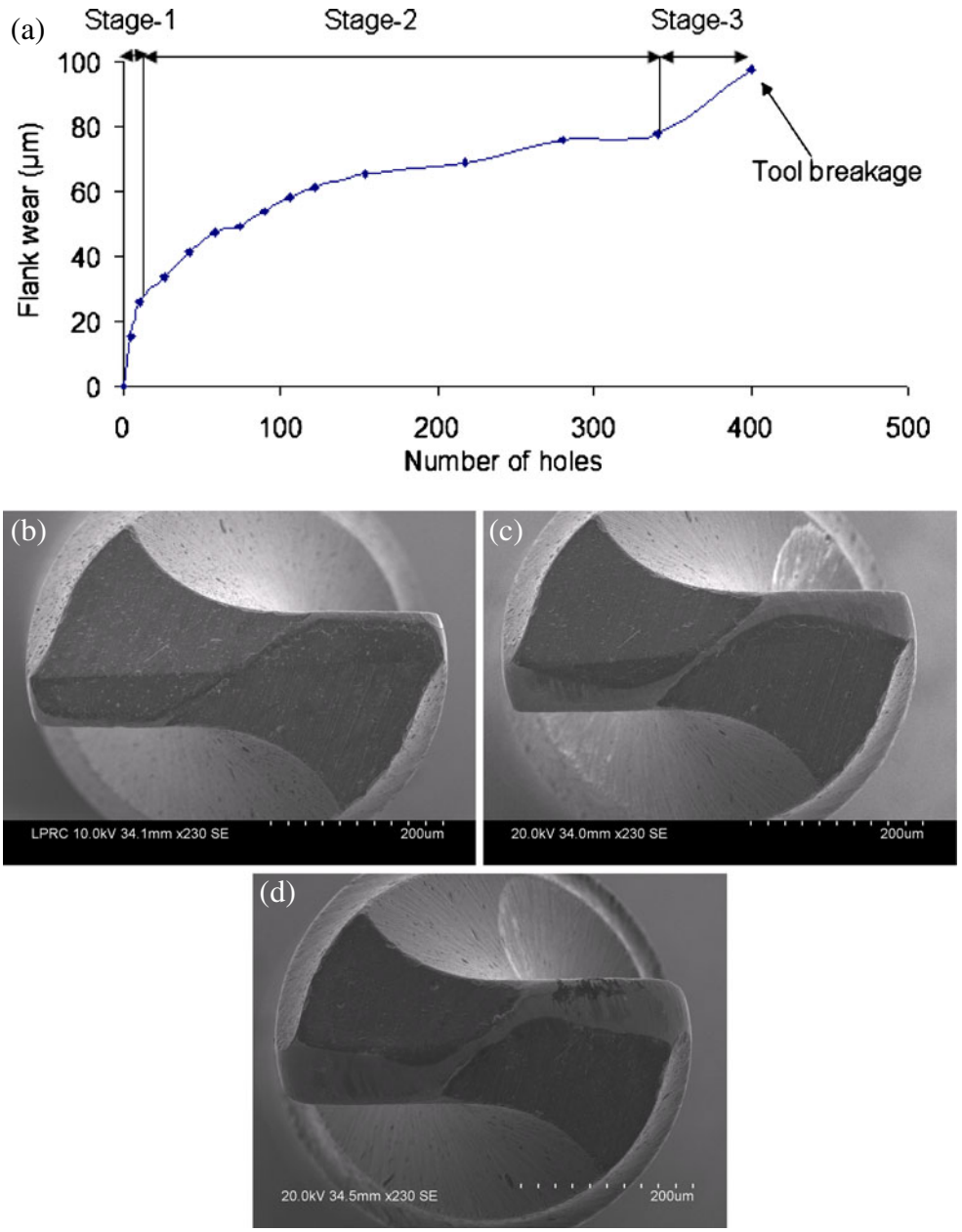


**Fig. 4** **a** The progress of flank wear with increasing numbers of holes drilled (feedrate=5 μm/rev and speed=3,000 rpm) alongside images of tool wear at **b** stage-1, **c** stage-2 and **d** stage-3

edge blunting (see Fig. 4d) and ultimately catastrophic failure of the tool. This information is very important because the marked stage-3 wear zone makes it easier for process monitoring.

Figure 5 shows the change of ratio of undeformed chip thickness to tool edge radius ($f/r_e$) with increasing numbers of holes drilled. Instantaneous values of tool edge radius were measured at regular intervals, and the corresponding $f/r_e$ ratios were plotted. Figure 5 shows that, as the tool edge radius increases, with increasing number of holes, $f/r_e$ ratio decreases. Observation of Figs. 4 and 5 shows that increased flank wear is accompanied by a reduced $f/r_e$ ratio. Furthermore, as the tool edge radius increases, the effective rake angle becomes more negative, and there is a greater ploughing action thereby resulting in increase of tool flank wear and plastic deformation.

Figure 6 shows the progression of $f/r_e$ ratio at various feed-rates with increasing number of holes. Since, $f/r_e$ ratio is below unity at lower feed-rates, i.e. 0.5, 2 and 5 μm/rev as compared with a high feed-rate of 8 μm/rev, greater ploughing could be expected. This indicates the presence of high tool wear in the low feed-rate regime and vice versa. Moreover, during tool wear, it was observed that, at lower feed-rates ($f/r_e<1$), the edge radius increased to a higher value as compared with higher $f/r_e$ ratios. This shows that lower values of $f/r_e$ ratios are associated with greater ploughing and result in higher wear rates. This fact is corroborated in the wear map presented later in Section 3.2.

During the course of this study, it has been observed that, when the instantaneous edge radius reaches six times the initial edge radius (3.5 μm), the tool wear accelerates exponentially. This represents the edge radius at the onset of stage-3 in Fig. 4. A similar edge radius of around 25 μm was reported near the end of tool life in the micro-milling of hardened die steel [34]. This implies that, when the ratio of initial edge radius to instantaneous edge radius reaches 16%, the effective rake angle becomes −49 degrees at a feed-rate of 5 μm/rev [35], and the cutting mechanism can be attributed to a shift towards a greater ploughing mode. At highly negative rake angles, the cutting forces are higher [36], which ultimately result in more tool wear and plastic deformation ahead of tool. These observations are interesting in developing a tool life criterion for micro-drills. It was also noted that the tool broke when this ratio of instantaneous edge radius to initial edge radius was 11%. This corresponds to a negative rake angle of −62 degrees [35].

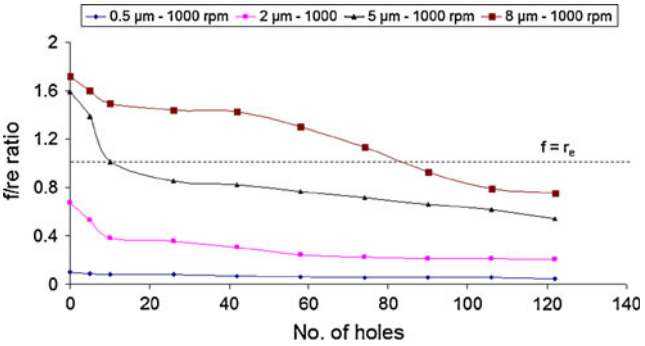


**Fig. 6** Variation of $f/r_e$ ratio with increasing number of holes drilled at various feed-rates

## 3.2 New wear map for micro-drilling

A two-dimensional map for flank wear is plotted as a dimensionless wear rate with speed along $X$ axis and feed-rate along the $Y$ axis in Fig. 7. A dimensionless wear parameter, $R$, which denotes a wear per unit cutting length, was plotted on the wear map. This was calculated using the parameter log (VB/$L$), where VB is the average flank wear and $L$ is the cutting distance. In machining, the wear rate parameter $R$ is usually negative. The higher the numeric magnitude of the $R$ value, the lower the wear rate and the more preferable is the machining zone/area.

This map was constructed for TiN-coated carbide tools on Inconel 718 alloy for wet cutting conditions. Four tool

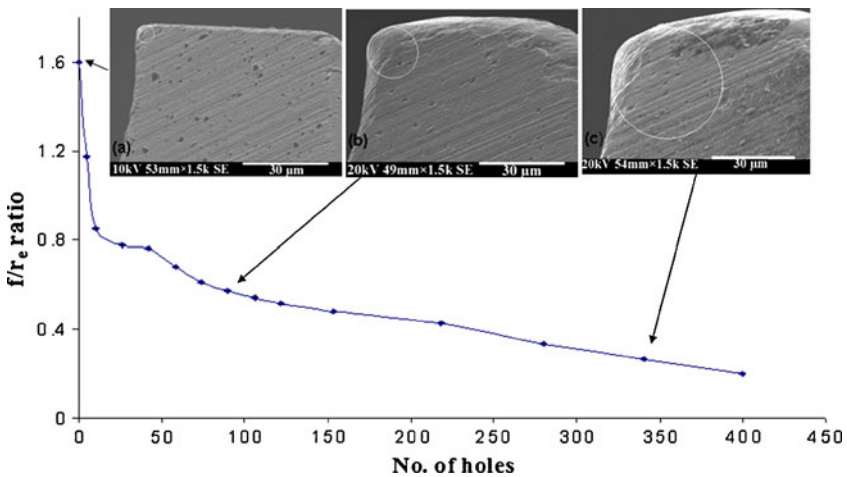


**Fig. 5** $f/r_e$ ratio progression with increasing number of holes (feed-rate=5 μm/rev and speed=3,000 rpm)

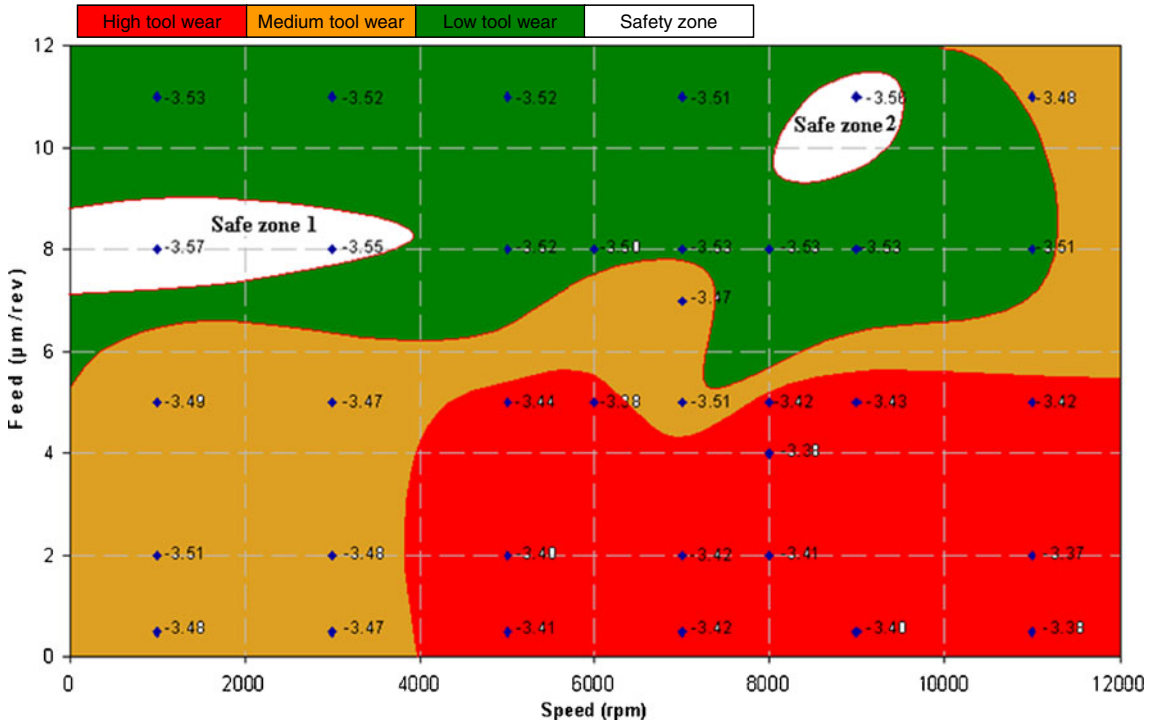


**Fig. 7** Flank face tool wear map (showing contours of constant $R$) for IN718 with a TiN-coated tool under wet cutting conditions

wear regions were identified (based on similar wear rates) by boundaries with a step length of 0.05 based on the change of wear rate, $R$. The values are separated as $R$ values greater than −3.45 constitute high tool wear regions, $\sim -3.45 > R > \sim -3.50$ signifies a medium tool wear region, $-3.50 > R > -3.55$ a low tool wear region and $R < -3.55$ a safe zone. The tool wear map obtained in this study exhibits two safe zones having non-dimensional wear rates ranging from −3.55 to −3.57. These safe regions lying in the vicinity of 8 μm/rev feed-rate and 3,000 rpm and 10 μm/rev feed-rate and 9,000 rpm. These regions indicate optimal cutting performance and significant economic advantages to the manufacturing industry.

The feasibility of mechanically drilling micro-holes in the aeroengine industry provides tooling flexibility over the established electrical discharge machining process. However, productivity is a major issue in terms of increasing material removal rate and thus reducing the cycle time in the process. This tool wear map provides a good reference in terms of productivity, especially in the two safe zones. It is notable that the productivity in terms of material removal rates increases by 600% moving from safety zone 1 to safety zone 2. This shows the optimum cutting parameters which correspond to the reduction of cycle time.

The comparison of EDX line scans showed that lower adhesion is associated with cutting conditions found in safe zone 2. One theory is that the contact phenomenon is different in the two zones. The detailed study of zone mechanisms is the subject of future study.

In order to ensure repeatability of results, additional experiments were conducted at various cutting conditions as shown on the map. The results obtained, further endorse the presence of similar tool wear rates in various tool wear zones. It is proposed that the wear map constructed during the course of this study could be used as a quick reference on the shop floor in the micro-drilling process. By using this map, the machinist can make necessary decisions on the choice of feeds and speeds to compromise between material removal rate and acceptable level of wear damage to micro-drills.

Using the tool wear map, it is noteworthy that high tool wear regions can be located either at lower undeformed chip thickness values (could be driven by strain hardening effects) or/and at high speeds (>4,000 rpm) due to rapid heating. The low tool wear zone and the safety zones do not occur at very low feed-rates which tend to support the well-established theory that the nickel alloys should be cut at feeds and depth of cut which minimise material strain hardening effects. In fact, the wear map suggests that, in micro-drilling, the feed-rate should not drop below 6 μm; otherwise, high wear to medium wear rates would be encountered. In general, it could be recommended that the micro-drilling process should be undertaken above 8 μm/rev and below 10,000 rpm. The upper limit of the feed will be set by tool strength.

### 3.3 Tool wear mechanism under wet drilling

In order to improve the machinability in the micro-drilling process for nickel-based super alloy, it is necessary to

investigate the underlying tool wear mechanism. In the case of the TiN-coated carbide tools used in this study, the tool wear mechanism starts from the abrasion of the TiN coating from the WC substrate. This abrasion process is followed by the cyclic adhesion of workpiece material onto the tool. Figure 8a shows significant adhesion of Ni, Cr and Fe elements on the tool extending further away from the cutting edge along the flank face. In addition, the EDX line scan in Fig. 8 shows that TiN coating is gradually abraded from the flank face, and the intensity of Ti and N increase gradually towards unworn area on the flank face. The data from Fig. 8 shows that the material transfer from the workpiece is associated with tool wear on the flank face. This adhesion of workpiece material on the flank face is followed by micro-chipping near the flank face. Abrasion and chipping were found to be the predominant tool wear mechanisms in earlier studies [18, 37].

## 4 Conclusions

The following conclusions can be drawn for the micro-drilling of nickel alloys:

1- Two regions of least wear rate were identified from the new wear map. The material removal rate can be increased by 600 % by moving from one of these regions to another. Thus, manufacturers/operators can choose one safe zone to extend drill life or the other to reduce the drilling cycle time.
2- The results suggest that the micro-drilling process should be undertaken above feed-rates of 8 μm/rev in order to reduce strain hardening effects and below 10,000 rpm to reduce thermal effects.
3- The progress of tool wear in the micro-drilling of nickel-based super alloys follows the three classical

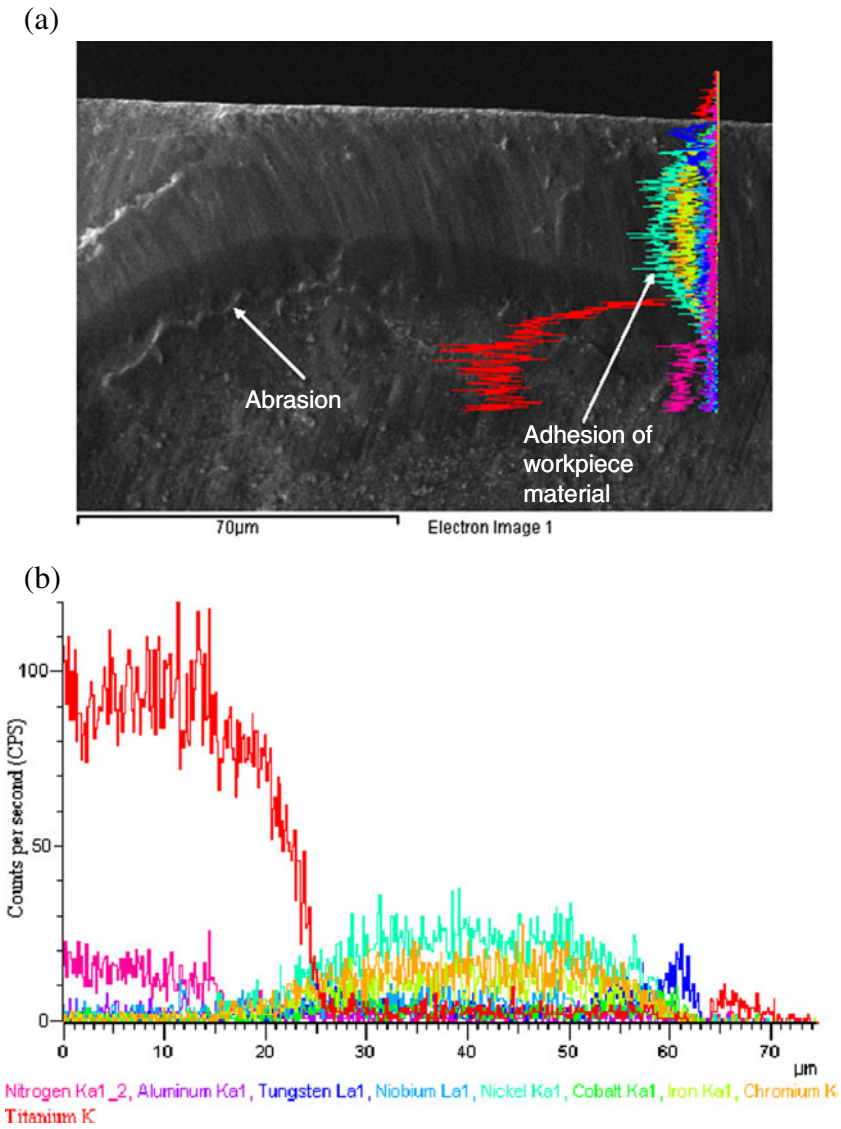


**Fig. 8** **a** Adhesion of work-piece material on the flank face. **b** EDX line scan from the cutting edge towards trailing edge across the flank face

stages. Stage-1 is characterised by rapidly increasing tool wear, and this is followed by stage-2 which has a near-uniform wear rate before stage-3 where rapid wear leads to tool breakage. This suggests that the onset of stage-3 should be identifiable in tool wear monitoring.

4- The useful drill life criterion corresponds to the point when the drill edge radius is about 20 μm which corresponds to 16% of the initial edge radius. This suggests that the tool life can be associated with the use of a blunt tool with highly negative rake angle.

5- More studies and tests are required by the authors and other independent researchers to explore the tool wear evolution pattern and the end of life criterion.

**Acknowledgements** The authors acknowledge the joint support offered by Engineering and Physical Sciences Research Council (EPSRC) and the Technology Strategy Board (TSB) under grants DT/E010512/1 and TP/6/MAT/6/K1028G, respectively.

## References

1. Ezugwu EO, Bonney J, Yamane Y (2003) An overview of the machinability of aeroengine alloys. J Mater Process Technol 134 (2):233–253
2. Ezugwu EO, Wang ZM, Okeke CI (1999) Tool life and surface integrity when machining Inconel 718 with PVD and CVD-coated tools. Tribol Trans 42(2):353–360
3. Arunachalam R (2000) Machinability of nickel-based high temperature alloys. Mach Sci Technol 4(1):127–168
4. Choudhury IA, El-Baradie MA (1998) Machinability of nickel-base super alloys: a general review. J Mater Process Technol 77 (1):278–284
5. Ezugwu EO, Lai CJ (1995) Failure modes and wear mechanisms of M35 high-speed steel drills when machining inconel 901. J Mater Process Technol 49(3):295–312
6. Komanduri R, Schroeder TA (1986) On shear instability in machining a nickel-iron base superalloy. Transactions of ASME Journal of Engineering for Industry 108:93–100
7. Chen YC (2003) Study on wear mechanisms in drilling of Inconel 718 superalloy. J Mater Process Technol 140(1):269–273
8. Lim SC, Ashby MF (1987) Wear-mechanism maps. Acta Metallurgica 35(1):1–24
9. Antoniou R, Subramanian C (1988) Wear mechanism map for aluminium alloys. Scr Metall 22(6):809–814
10. Lim SC, Lee SH, Liu YB, Seah KHW (1993) Wear maps for uncoated high-speed steel cutting tools. Wear 170(1):137–144
11. Lim CYH, Lau PPT, Lim SC (2001) The effects of work material on tool wear. Wear 250:344–348
12. Lim CYH, Lau PPT, Lim SC (2001) Work material and the effectiveness of coated tools. Surface & Coatings Technology 146–147:298–304
13. Jaffery SI, Mativenga PT (2009) Assessment o the machinability of Ti-6Al-4 V alloy using the wear map approach. Int J Adv Manuf Technol 40:687–696
14. Lee K, Dornfeld DA (2005) Micro-burr formation and minimization through process control. Precis Eng 29(2):246–252
15. Zhang MZ, Liu YB, Zhou H (2001) Wear mechanism maps of uncoated HSS tools drilling die-cast aluminum alloy. Tribol Int 34 (11):727–731
16. Wang J, Liu YB, An J, Wang LM (2008) Wear mechanism map of uncoated HSS tools during drilling die-cast magnesium alloy. Wear 265(5–6):685–691
17. Sharman ARC, Amarashighe A, Ridgway K (2008) Tool life and surface integrity aspects when drilling and hole making in Inconel 718. J Mater Process Technol 200(1):424–432
18. Imran M, Mativenga PT, Kannan S, Novovic D (2008) An experimental investigation of deep-hole microdrilling capability for a nickel-based superalloy. Proceedings of the Institution of Mechanical Engineers; Part B; Journal of Engineering Manufacture 222(12):1589–1596
19. Imran M, Mativenga P T, Kannan S, (2010) An investigation into the effects of tool geometry in micro drilling process for nickel based superalloy. The 5th International Conference on Micro-Manufacturing ICOMM / 4 M, April 5–8, Madison, WI, USA: 85–93.
20. Xu SL, Watanabe TA, Yoshida K (1989) Micro-drilling of a new Ni-based superalloy. Chiba daigaku kogakubu kenkyu ho 41(1):31–41
21. Klocke F, Gerschwiler K, Abouridouane M (2009) Size effects of micro drilling in steel. Production Engineering Research 3(1):69–72
22. Liu X, DeVor RE, Kapoor SG, Ehmann KF (2004) The mechanics of machining at the microscale: assessment of the current state of the science. J Manuf Sci Eng 126(4):666–678
23. Chae J (2006) Investigation of micro-cutting operations. International Journal of Machine Tools & Manufacture 46(3):313–332
24. Nakayama K, Tamura K (1968) Size effect in metal cutting force. Transactions of ASME, Journal of Engineering for Industry 90:119–126
25. Lucca D A, Seo Y W, Rhorer R L, (1992) Effect of the tool workpiece interface on energy dissipation in ultra-precision machining of aluminium. Proceedings of Seventh Annual Meeting of the American Society for Precision Engineering.
26. Lucca DA, Rhorer RL, Komanduri R (1991) Energy dissipation in the ultraprecision machining of copper. CIRP Annals - Manufacturing Technology 40(1):69–72
27. Moriwaki T, Okuda K (1989) Machinability of copper in ultra-precision micro diamond cutting. CIRP Annals - Manufacturing Technology 38(1):115–118
28. Kudla L (2001) Influence of feed motion features on small holes drilling process. J Mater Process Technol 109(3):236–241
29. Li R, Hegde P, Shih AJ (2007) High-throughput drilling of titanium alloys. International Journal of Machine Tools & Manufacture 47(1):63–74
30. Schulz H, Moriwaki T (1992) High-speed machining. CIRP Annals-Manufacturing Technology 41(2):637–643
31. Aramcharoen A, Mativenga PT, Yang S, Cooke KE, Teer DG (2008) Evaluation and selection of hard coatings for micro milling of hardened tool steel. International Journal of Machine Tools and Manufacture 48(14):1578–1584
32. Kudla LA (2006) Deformations and strength of miniature drills. Proceedings of the Institution of Mechanical Engineers, Part B: Journal of Engineering Manufacture 220(3):389–396
33. Rao IV, Lal GL (1977) Tool life at high cutting speeds. International Journal of Machine Tool Design and Research 17 (4):235–243
34. Aramcharoen A, Mativenga P T, (2008) Tool wear modes in micro/mesoscale milling of hardened die steel. Proceedings of the 3 rd International CIRP High Performance Cutting Conference, Dublin: 179–188.
35. Bissacco G, Hansen HN, Slunsky J (2008) Modelling the cutting edge radius size effect for force prediction in micro milling. CIRP Annals-Manufacturing Technology 57(1):113–116
36. Komanduri R (1971) Some aspects of machining with negative rake tools simulating grinding. International Journal of Machine Tool Design and Research 11(3):223–233
37. Liao YS, Shiue RH (1996) Carbide tool wear mechanism in turning of Inconel 718 superalloy. Wear 193:16–24